NANO LETTERS

2008
Vol. 8, No. 1
162−167

Hydrogen Storage in Carbon Nanotubes through the Formation of Stable C–H Bonds

Anton Nikitin,[†] Xiaolin Li,[‡] Zhiyong Zhang,[‡] Hirohito Ogasawara,[†] Hongjie Dai,[‡] and Anders Nilsson*[,†,§]

Stanford Synchrotron Radiation Laboratory, 2575 Sand Hill Road, Menlo Park, California 94025, Department of Chemistry, Stanford University, Stanford, California 94305, and FYSIKUM, Stockholm University, Albanova University Center, S-10691 Stockholm, Sweden

Received September 10, 2007; Revised Manuscript Received November 13, 2007

ABSTRACT

To determine if carbon-based materials can be used for hydrogen storage, we have studied hydrogen chemisorption in single-walled carbon nanotubes. Using atomic hydrogen as the hydrogenation agent, we demonstrated that maximal degree of nanotube hydrogenation depends on the nanotube diameter, and for the diameter values around 2.0 nm nanotube-hydrogen complexes with close to 100% hydrogenation exist and are stable at room temperature. This means that specific carbon nanotubes can have a hydrogen storage capacity of more than 7 wt % through the formation of reversible C–H bonds

To realize hydrogen-powered transportation, it is necessary to find ways to store hydrogen on-board efficiently and safely. One of the possible ways for storage is hydrogen adsorption on a medium capable of easily and reliably absorbing and releasing large amounts of hydrogen. Carbon nanotubes are possible candidates for such a medium, and mechanisms of hydrogen storage through both physisorption and chemisorption have been proposed. While the physisorption of H_2 species can provide only about 1 wt % of hydrogen storage capacity at room temperature,[1] it was shown experimentally that hydrogen forms stable C−H bonds on the single-walled carbon nanotube (SWCN) surfaces[2] and theoretically that chemisorption can provide a hydrogen storage capacity up to 7.7 wt %.[1] Nevertheless, the existence of the fully hydrogenated SWCN and their stability should be demonstrated experimentally before any other steps toward the development of a nanotube-based hydrogen storage system are taken.

In the present study we used in situ atomic hydrogen treatment of the nanotube films to separate the hydrogenation from the molecular hydrogen dissociation process. Atomic force microscopy (AFM) was used to characterize the size distribution of the nanotubes, and X-ray photoelectron spectroscopy (XPS) was used to determine the degree of hydrogenation. The latter provides information about the presence of the C−H bonds through the C1s core level shift and also allows for quantifying the number of such bonds per carbon atom.[2] We found that depending on the nanotube diameter different hydrogenation degrees can be reached before hydrogenated nanotubes become unstable and decompose. We also show that for SWCN with diameter around 2.0 nm almost 100% hydrogenated nanotubes are stable at room temperature that is equivalent to ∼7 wt % of hydrogen storage capacity. We found that most of the C−H bonds formed on the nanotube surface dissociate in the temperature range between 200 and 300 °C and that hydrogen desorption is mainly controlled by reaction kinetics due to large activation barriers for H_2 formation from stable H pairs adsorbed on the SWCN.

Two different types of as-grown SWCN thin films (type 1 and type 2) were used in this study. Studied films were grown on a silicon wafer covered with a thin layer of native oxide using different chemical vapor deposition techniques. For type 1 (T1) film, the catalyst for the growth was made by sonification of a mixture of 50 mg Degussa Aerosil 380 silica, 4.5 mg of cobalt acetate, 3.1 mg of iron acetate, and 0.77 mg of molybdenum acetate in ethanol for 2 h and was spin-coated on the surface of the wafer at 3000 rpm. The SWCN films were grown by flushing a 1in. quartz tube containing the prepared wafer with 1000 sccm of forming gas (3% H_2 in argon) and 1000 sccm of H_2 for 10 min, heating up to 850 °C in 1000 sccm of forming gas and 1000

* Corresponding author. E-mail: nilsson@slac.stanford.edu. Phone: +1 650 926 2233. Fax: +1 650 936 4100.
[†] Stanford Synchrotron Radiation Laboratory.
[‡] Stanford University.
[§] FYSIKUM, Stockholm University, Albanova University Center.

10.1021/nl072325k CCC: $40.75
Published on Web 12/19/2007

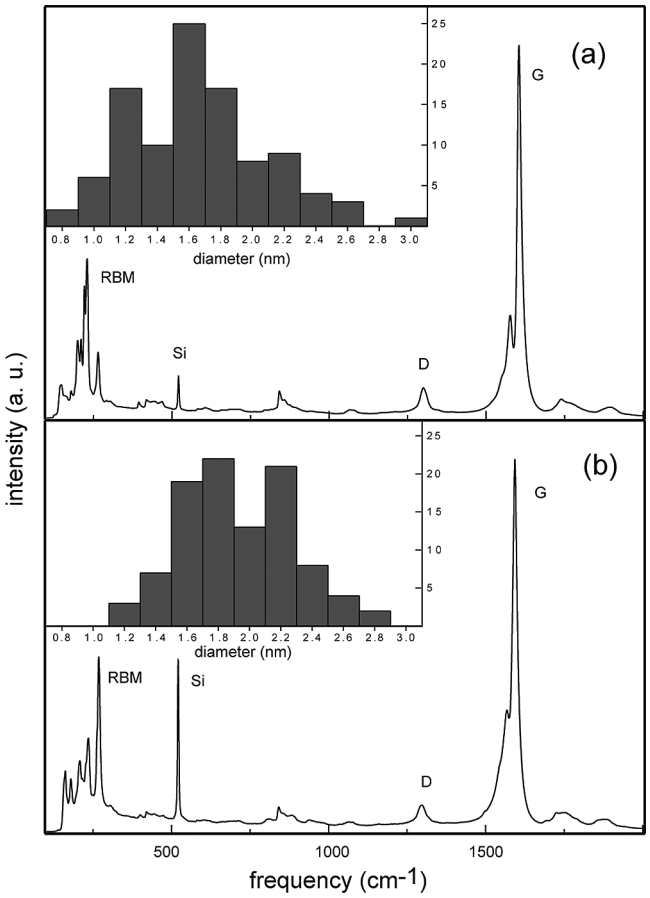

Figure 1. Raman spectra and histograms (diameter distributions) obtained from AFM measurements for T1 (a) and T2 (b) samples.

sccm of H_2, then flushing with 1000 sccm of forming gas and 1000 sccm of argon for 5 min. After this, 1000 sccm of forming gas bubbling through the ethanol and 1000 sccm of argon were flowed for 5 min at 850 °C, followed by cooling down in 1000 sccm of forming gas and 1000 sccm of H_2. Type 2 (T2) films were prepared according to the procedure described in ref 2.

The low *D* to *G* band intensity ratio in the Raman spectra of such films, which were measured using a Renishaw micro-Raman instrument with 785 nm excitation laser wavelength, indicates their high quality (low concentration of amorphous carbon and defects) (see Figure 1). Scanning electron microscopy also showed that the nanotubes did not cover the substrate completely and partly were found in bundles. The T1 film covered ~90% of the substrate surface, and the T2 film covered ~40%. To determine the SWCN diameter distribution in the T1 and T2 films, detailed AFM measurements were performed using specially prepared samples grown at catalyst-patterned Si substrate. Samples were made by a well-developed technique introduced in ref 3 with 5×5 μm^2 catalyst pattern, and AFM images were taken in tapping mode using an ex situ Nanoscope IIIa multimode instrument. The results of the AFM investigation showed that the size distribution of the SWCN in the T1 film had an average nanotube diameter equal to 1.6 nm and in the T2 film of 2.0 nm (see insets in Figure 1a,b).

The XPS studies were performed at beamline 5-1 at the Stanford Synchrotron Radiation Laboratory (SSRL). The energy resolution of the XPS spectra was better than 0.1 eV. An atomic hydrogen beam was produced by thermal cracking of molecular hydrogen in a W capillary.[4] Typical pressure in the chamber during H treatment was 5×10^{-7} Torr with the distance between sample and the H source at 25 cm, and the W capillary temperature was above 2000 °C. The SWCN films were cleaned by careful annealing up to 750 °C with an operating pressure below 1×10^{-9} Torr before in situ atomic hydrogen treatment. The XPS spectra showed no signals from impurities and residual metal catalysts, Fe, Co, or Mo, in the SWCN films. Also no influence of charging on the measured XPS spectra was observed.

The XPS C1s chemical shifts were calculated in the framework of density functional theory[5] using the StoBe software package.[6] The structures of the pristine nanotubes and nanotubes with adsorbed hydrogen atoms were obtained from molecular dynamics optimization using the adaptive intermolecular reactive empirical bond order potential.[7]

Reaction pathways and transition states were located by the climbing image nudged elastic band (NEB) method[8] using VASP[9,10] with the local density approximation of Ceperley and Alder[11] as parametrized by Perdew and Zunger.[12] Blöchl's projector augmented wave (PAW) potentials[13] were used for the ion-electron interactions. The PAW potentials were from the database provided through VASP, and the default energy cutoffs were used. At least five k-points in the direction of the tube axis were used in the simulations with a supercell size of $14.264 \times 14.264 \times 14.264$ Å.

The XPS spectra for the T1 sample with increasing hydrogen dosage are shown in Figure 2. From these data, we see that H treatment of the T1 film causes the formation of a second peak (denoted by peak 2) in the C1s line separated by ~0.7 eV from the peak of the pure carbon nanotubes (Figure 2, plot b), similar to previous observations.[2] The same chemical shift of the C1s line was also observed for graphite under H treatment.[14,15] This second spectral feature appears due to carbon atoms coordinated with hydrogen, and its intensity is directly proportional to the number of the C−H bonds formed and therefore corresponds to the nanotube hydrogenation degree.[2] The relative intensities of peaks 1 and 2 in the spectrum measured after the first dose of H treatment for the T1 sample correspond to 30 ± 5 % hydrogenation of SWCN, and additional H treatment does not lead to any dramatic changes in the spectral shape (see plots b, c, and d, Figure 2). The relative ratio between peak 1 and peak 2 intensities stays almost the same (see inset, Figure 2), while the peak full width at half-maximum increases and the total intensity of the C1s line decreases with the increasing H treatment dose. Such spectral behavior indicates that as soon as ~30% hydrogenation of nanotubes in sample T1 is archived additional H treatment causes etching of the SWCN film.

The scenario of the T2 sample is rather different. We observe that H treatment also causes the appearance of peak 2 in the C1s spectra and a decrease of the intensity of peak 1 (see Figure 3-1, plot b), similar to what was observed for

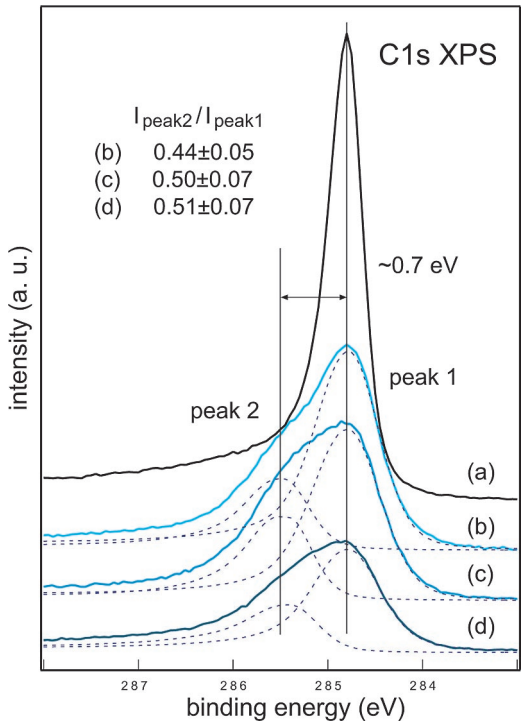

Figure 2. XPS spectra of hydrogenation sequences of the T1 sample measured at $E_{h\nu} = 350$ eV. Spectra are normalized by the background. (a) Clean T1 sample; (b) H-treated T1 sample; (c) H-treated T1 sample with 2 times higher H dose than in (b); and (d) H-treated T1 sample with 4 times higher H dose than in plot b. Inset: peak 2 to peak 1 intensity ratios for different spectra.

the T1 sample. Additional H treatment leads to further decrease of peak 1 (see Figure 3-1, plot c), and higher doses of H result in almost complete elimination of peak 1 with the appearance of an additional spectral feature (peak 3) (see Figure 3-1, plot d). The appearance of the third peak is different from what we observed for sample T1. Taking into consideration that the total intensity of the C1s line does not change to any large degree upon H exposure, we can conclude that SWCN in the T2 sample does not decompose with modest H treatments.

Such hydrogen-induced nanotube decomposition or "unzipping" was predicted theoretically[16] and observed experimentally.[17,18] Both theoretical[16] and experimental[17,18] studies show that nanotubes with larger diameter, due to their overall lower reactivity as defined by the smaller curvature, are more resistant to the hydrogenation-induced etching in comparison with smaller diameter SWCN. Also, it was demonstrated[18] that semiconducting SWCN are more stable under H plasma treatment than metallic ones. Our results show that T1 and T2 SWCN samples behave differently under H treatment: for the T1 sample ~30% hydrogenation makes nanotubes unstable with subsequent material etching and for the T2 sample almost 100% hydrogenated nanotubes are stable. We see from the nanotube diameter distributions (see Figure 1) that for the T1 sample the average diameter is around 1.6 nm whereas it is around 2.0 nm for the T2 sample. This difference in average diameter can be one of the reasons for the differences observed in the etching scenarios for T1 and T2 samples. Another possibility could be different chirality distributions in the T1 and T2 samples that could not be characterized in the current study.

However, upon extremely long exposure of the T2 sample (large diameters) as shown in Figure 3-1, plot e, the C1s total intensity starts to decrease, indicating that fully hydrogenated SWCN of T2 type can also be etched with atomic hydrogen when we have reached nearly 100% hydrogenation. In this case, almost every new H atom reaching the SWCN surface interacts with a CH group. Although there is an energy barrier to convert the CH group into CH_2, there is a probability that it can be overcome by H atoms with sufficient kinetic energy. The CH_2 groups are very unstable in the presence of additional H species and are converted through the breakage of C−C bonds, resulting in the formation of methane that directly desorbs.[19]

We also obtained AFM images of the same tubes before and after hydrogenation using catalyst-patterned samples. H treatment was performed in a separate ultrahigh vacuum chamber, and the AFM images of the hydrogenated samples were measured ex situ in air. Figure 4 shows some typical tapping mode AFM images of the nanotubes with different diameters before and after hydrogenation. We see that hydrogenation causes an increase of the nanotube diameter which was first observed in ref 17. It should be pointed out that the same H treatment causes a much higher relative diameter increase for the nanotubes with small diameters than for the nanotubes with larger ones (see Figure 4). We also observed cuts for the thin nanotubes while thick nanotubes stayed intact after the same H treatment (see Figure 4c,d). This observation provides further evidence of the higher resistance of larger diameter SWCN toward H treatment-induced etching.

The nanotubes in the samples were partially in bundles. As a result, not all of the SWCN were on the surface of the studied films and could be directly exposed to the atomic hydrogen beam. To distinghuish the hydrogenation process of the nanotubes in the outer layer of the bundles with nanotubes lying deeper in the bundles for the T2 sample (large diameters), XPS C1s measurements were performed at different photon energies during the H treatment sequence (see Figure 3). Changing the X-ray excitation energy $E_{h\nu}$ causes variations of the C1s photoelectron kinetic energy E_{kin} and their inelastic mean free path λ, therefore resulting in differences in the effective probing depths of the XPS measurements. In the case of graphite with $E_{h\nu} = 350$ eV, E_{kin} is 65 eV, and λ is 0.48 nm whereas for $E_{h\nu} = 700$ eV, E_{kin} is 415 eV, and λ is 0.95 nm.[20] As a result, the XPS probing depth (the thickness of the sample accounting for 75% of the signal) for $E_{h\nu} = 700$ eV is 2 times larger than for $E_{h\nu} = 350$ eV. We therefore attribute measurements performed at $E_{h\nu} = 350$ eV as containing mainly the intensity from carbon atoms in nanotubes lying in the outer layer of the bundles (on the surface of the studied film) and measurements performed at $E_{h\nu} = 700$ eV as ones containing both information from outer layer and layers lying deeper in the bundles that are less exposed to the direct H beam.

Figure 3 shows that for the T2 sample (large diameters) only spectra measured after the first H treatment at the two

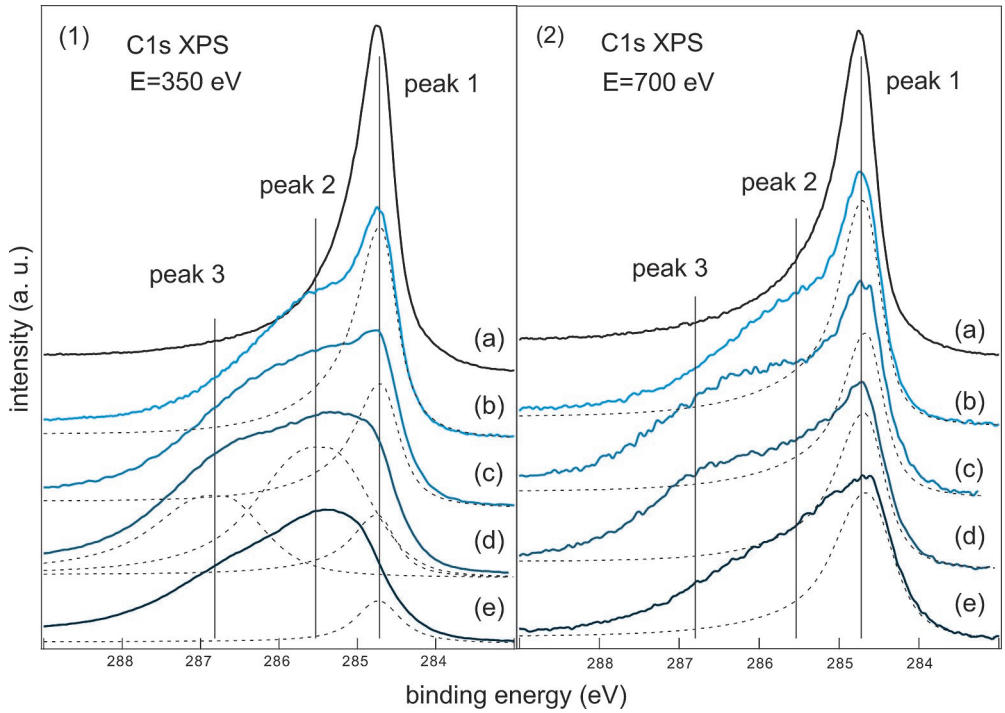

Figure 3. XPS spectra of hydrogenation sequences of the T2 sample measured at $E_{h\upsilon} = 350$ eV (1) and at $E_{h\upsilon} = 700$ eV (2). Spectra are normalized by background. (a) Clean T2 sample; (b) H-treated T2 sample; (c) H-treated T2 sample with 9 times higher H dose than in plot b; (d) H-treated T2 sample with 26 times higher H dose than in plot b; and (e) H-treated T2 sample with 46 times higher H dose than in plot b. Plot d in part (1) shows one of the possible decompositions of the C1s spectrum where peak 2 and peak 3 components have the same asymmetry parameters as peak 2 for the plot b in part (1) (decomposition is not shown). The peak intensity uncertainty is 10%.

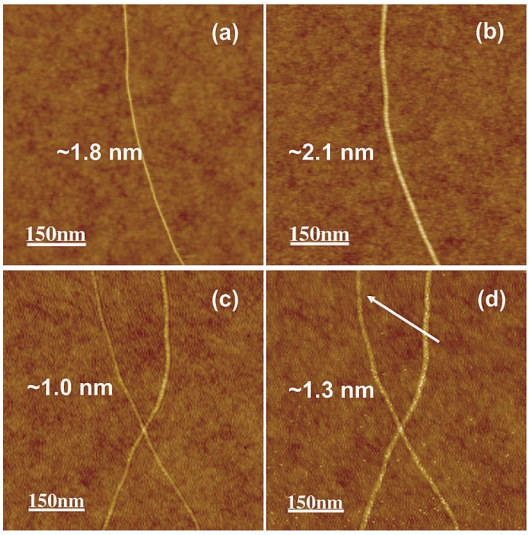

Figure 4. AFM images of the same tubes before and after hydrogenation. (a) Before hydrogenation, a SWNT with the diameter of ~1.8 nm; (b) diameter of the tube in panel a increased to ~2.1 nm after hydrogenation; (c) before hydrogenation, a SWNT with diameter of ~1.0 nm; (d) the tube in panel c is cut after hydrogenation (marked with arrow) and diameter of the tube increased to ~1.3 nm.

different photon energy give a similar spectral shape (see Figure 3-1, plot b and Figure 3-2, plot b) indicating a uniform hydrogenation of nanotubes in the bundles. The decomposition of these spectra into two components[2] shows that the relative intensities of peaks 1 and 2 are almost the same for spectra at $E_{h\upsilon} = 350$ eV and $E_{h\upsilon} = 700$ eV and correspond to 40 ± 5 % hydrogenation of the nanotubes. Additional H treatment causes a larger change in the shape of the spectra measured at $E_{h\upsilon} = 350$ eV than for spectra measured at $E_{h\upsilon} = 700$ eV. These observations show that the hydrogenation is uniform across SWCN film under H beam up to this point of hydrogenation. Additional H treatment leads to an increase of the hydrogenation degree of the nanotubes located only in the outer layer of the bundles resulting in a nonuniform hydrogenation across the SWCN film.

According to previous theoretical calculations,[21] for H atoms adsorbed on the SWCN surface it is energetically more favorable to form pairs. For example, the most favorable configuration of the pair of H atoms chemisorbed on the (8,0) nanotube surface is C2C3 (see Figure 5-3). Also theoretical calculations for the diffusion paths[21] showed that single H atoms can diffuse more easily (the diffusion barrier is ~0.7 eV), while the energetically favorable H pairs have a much higher barrier for the diffusion (~1.3 eV). As a result, at low H coverage each additional H atom adsorbing at the nanotube surface can easily diffuse until it meets another H atom and forms a stable H pair. As the hydrogen coverage reaches a high value, most of the H atoms form stable pairs just after adsorption from H beam, and as a result H diffusion along nanotube surface decreases. So the increase of the hydrogenation degree takes place only on the nanotubes located in the outer layer of the bundles that are directly exposed to the H beam.

As mentioned above, the C1s line of the highly hydrogenated T2 sample possesses an additional spectral feature denoted as peak 3. Curve fitting of the spectrum shows (see Figure 3-1, plot d) that peak 3 is separated by ~2.1 eV from

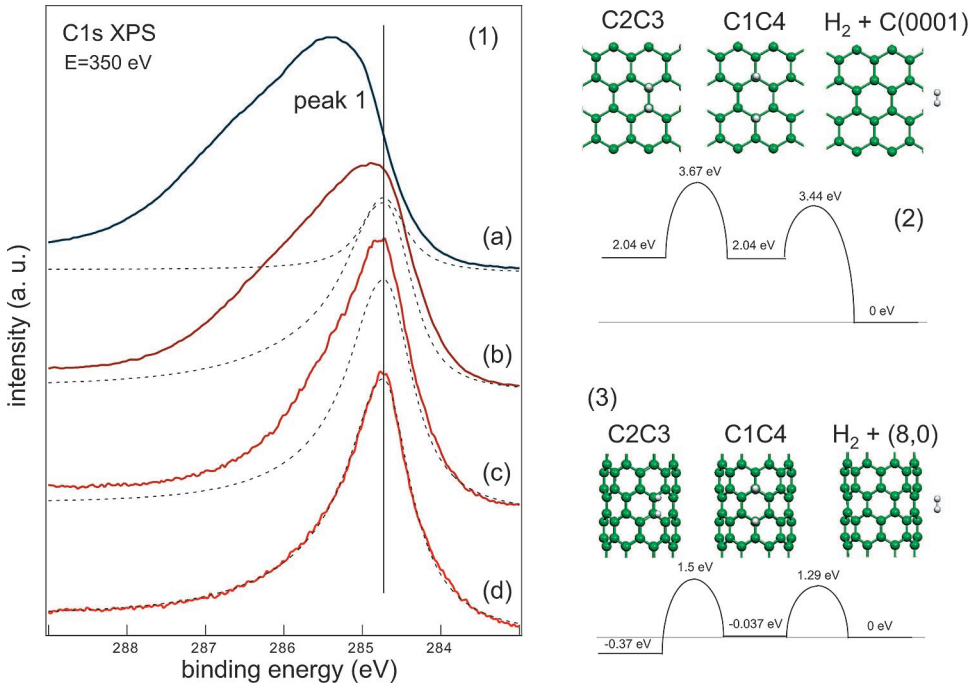

Figure 5. (1) XPS spectra of annealing sequences of the highly hydrogenated T2 sample measured at $E_{h\nu} = 350$ eV. (a) H-treated sample; (b) sample annealed at 200 °C; (c) sample annealed at 300 °C; and (d) sample annealed at 550 °C. (2) Hydrogen desorption diagram for the hydrogen adsorbed at the graphite C(0001) surface from ref 26. (3) Calculated hydrogen desorption diagram for the hydrogen adsorbed at the surface of (8,0) SWCN ($d = 0.63$ nm).

the main C1s peak and has a shape similar to peak 2. Our theoretical calculations show that the formation of CH_n groups on the nanotube surface where $n > 1$ can only cause a maximum chemical shift of 0.9 eV, and therefore a different explanation is required. Theoretical[22,23] and experimental[17] studies indicate that nanotube hydrogenation causes an increase of the band gap and nanotube resistance. We anticipate that nanotubes in the outer bundle layer are converted by the hydrogenation process more toward an insulator. As a result the core hole formed in the photoionization process loses the metallic electron screening channel and the final state of the photoelectron process changes.[24] This results in an additional shift of the C1s peak toward higher binding energies for a less screened final state. This has previously been observed in the case of *n*-octane adsorbed on a clean metal substrate where the elimination of the metallic electron screening channel in the growth of multilayers causes an additional C1s peak shift on the order of 0.8 eV in comparison with the monolayer, which is in direct contact with the metal.[25]

The decomposition of the spectra measured of the T2 sample (large diameters) after maximal dose of the H treatment shown in Figure 3-1, plot d, allows for a direct evaluation of the degree of nanotube hydrogenation by calculating the ratio between the intensity of C1s peak components from C−H-bonded carbon (peak 2 and peak 3) to the total intensity. By using the spectrum measured at 350 eV, providing higher surface sensitivity, it is possible to estimate the hydrogenation degree of the SWCN in the outer layer of the studied film. The intensity ratio between peaks 1, 2, and 3 is 1:4:6. Considering that at least one hydrogen is bonded to each carbon atom that contributes to peaks 2 and 3, this decomposition of spectrum corresponds to 91 ± 5 % hydrogenation or 7.0 ± 0.4 wt % of hydrogen storage capacity. Anticipating that part of the intensity in peak 1 could be due to the signal from the nanotubes lying deeper in the film, we conclude from the above results that for the SWCN with diameters around 2.0 nm almost 100% hydrogenated nanotubes exist and are stable at ambient temperatures.

The hydrogen desorption from hydrogenated T2 SWCN film was studied by temperature-dependent X-ray photoelectron spectra. Figure 5-1 shows C1s spectra for the hydrogenated T2 SWCN film recorded after in situ annealing at different temperatures. We observed that annealing at 200 °C causes the peak 1 intensity to increase, while annealing at 300 °C causes almost a complete diminishing of the intensity in the energy range of peaks 2 and 3. Such behavior of the spectra during annealing indicates that more than two-thirds of the C−H bonds in the hydrogenated SWCN film dissociate at a temperature below 300 °C. From this observation, we conclude that chemisorbed hydrogen desorbs from the SWCN surface at temperatures in the range between 200 and 300 °C.

We calculated the desorption pathway of hydrogen adsorbed at the surface of (8,0) SWCN (see Figure 5-3). Comparing these results with the desorption pathway shown in Figure 5-2, calculated for graphite by ref 26, we see that there is only a small difference in the desorption barrier but a large difference in the adsorption energetics between the (8,0) nanotube with a diameter of 0.67 nm, and graphite, which can be considered as a nanotube with infinite diameter. These two cases represent two extremes with either a very small or infinitely large diameter. In the case of the (8,0)

SWCN, the most stable C2C3 configuration of the adsorbed hydrogen has an energy gain of 0.37 eV relative to the isolated nanotube and molecular H_2. This configuration is separated by a kinetic barrier of ~1.5 eV from the C1C4 configuration (see Figure 5-3). In the case of graphite, the same hydrogen pair is in a metastable state with an energy ~2 eV above the isolated units with a kinetic barrier equal to 1.6 eV that controls the desorption of the hydrogen (see Figure 5-2). In this sense, the hydrogen desorption temperature is defined by the desorption kinetics through the height of the desorption barrier, which is more or less constant for nanotubes with different diameters. The enthalpy related to adsorption and desorption is defined by the energy difference between the adsorbed hydrogen pair at C2C3 relative and the separated H_2 molecule and SWCN. For efficient hydrogen storage, the hydrogen adsorption/desorption process should be energetically "neutral" (no energy is consumed in the adsorption process, no energy is released in the desorption process), and from this point of view the free energy (taking into account the adsorption energy and the entropic effect of the free H_2) of the C2C3 pair should be close to 0 and only a nonzero desorption barrier keeps the system stable. Taking into consideration the theoretically predicted linear C−H bond energy dependence on the curvature of the nanotubes,[27] there are nanotubes with specific diameters possessing hydrogen desorption/adsorption energetics close to being energy neutral. In this case the amount of energy necessary to desorb hydrogen is defined only by the height of desorption barrier equal to ~1.5 eV. But this energy can be recuperated in the desorption process through the thermal energy exchange between the desorbed hot hydrogen gas and nanotubes and does not necessarily create serious energetic overhead, which can decrease the energy efficiency of the whole process.

To be able to use hydrogen chemisorption in SWCN as a hydrogen storage mechanism for technological applications, we need to find a viable way to form H−SWCN complexes. A possible way to do this is to use the spillover process.[28] In this case, the H_2 molecules dissociate at the surface of catalyst nanoparticles deposited on the nanotube surface and H radicals spill over from the catalyst to the surface of the nanotubes and form C−H bonds. It has been shown that the presence of Pt nanoparticles inside nanotube material gives a 5-fold increase of the hydrogen uptake.[29] This experimental result directly indicates that a spillover process exists for SWCN covered with a catalyst. We can thereby envisage that by choosing nonbundled nanotubes with appropriate diameter distribution, optimizing the nanostructure of deposited catalyst, and by choosing appropriate hydrogenation temperature to enhance H species diffusion along nanotube surface we can use the spillover process to form the H−SWCN complexes without compromising the hydrogen weight capacity of the material.

We found that, depending on the diameter of the nanotubes, different hydrogenation degrees can be reached before nanotubes become unstable and decompose. For SWCN with diameters around 2.0 nm, almost 100% hydrogenation can be obtained and hydrogenated nanotubes are stable at room temperature. This corresponds to 7 wt % of hydrogen storage capacity that is higher than DOE FreedomCAR Hydrogen Storage Technologies Roadmap goal for 2010 (6 wt %).[30] The hydrogen desorption temperature is between 200 and 300 °C and is mainly controlled by kinetics of the desorption reaction due to large activation barriers for H_2 formation from stable H pairs adsorbed on the SWCN.

Acknowledgment. This work was supported by the Global Climate and Energy Project operated by Stanford University and carried out at the Stanford Synchrotron Radiation Laboratory, a national user facility operated by Stanford University on behalf of the U.S. Department of Energy, Office of Basic Energy Sciences.

References

(1) Li, J.; Furuta, T.; Goto, H.; Ohashi, T.; Fujiwara, Y.; Yip, S. *J. Chem. Phys.* **2003**, *119*, 2376−2385.
(2) Nikitin, A.; Ogasawara, H.; Mann, D.; Denecke, R.; Zhang, Z.; Dai, H.; Cho, K.; Nilsson, A. *Phys. Rev. Lett.* **2005**, *95*, 225507.
(3) Kong, J.; Soh, H. T.; Cassell, A.; Quate C. F.; Dai. H. *Nature* **1998**, *395*, 878−881.
(4) Eibl, C.; Lackner, G.; Winkler, A. *J. Vac. Sci. Technol., A* **1998**, **16**, 2979−2989.
(5) Slater, J. C.; Johnson, K. H. *Phys. Rev. B* **1972**, *5*, 844−853.
(6) Hermann, K.; Pettersson, L. G. M.; Casida, M. E.; Daul, C.; Goursot, A.; Koester, A.; Proynov, E.; St-Amant, A.; Salahub, D.R. Contributing authors: Carravetta, V.; Duarte, H.; Godbout, N.; Guan, J.; Jamorski, C.; Leboeuf, M.; Malkin, V.; Malkina, O.; Nyberg, M.; Pedocchi, L.; Sim, F.; Triguero, L.; Vela, A. *StoBe-deMon*, version 2.0; StoBe Software, Berlin, 2002.
(7) Stuart, S., Tutein, A.; Harrison, J. A. *J. Chem. Phys.* **2000**, *112*, 6472−6486.
(8) Jonsson, H.; Mills, G.; Jacobsen, K. W. In *Classical and Quantum Dynamics in Condensed Phase Simulations*; Berne, B. J., Ciccotti, G., Coker D. F., eds.; World Scientific: Singapore, 1998.
(9) Kresse, G.; Hafner, J. *Phys. Rev. B* **1993**, *47*, 558−561.
(10) Kresse, G.; Furthmuller, J. *Phys. Rev. B* **1996**, *54*, 11169−11186.
(11) Ceperley, D. M.; Alder, B. J. *Phys. Rev. Lett.* **1980**, *45*, 566−569.
(12) Perdew, J. P.; Zunger, A. *Phys. Rev. B* **1981**, *23*, 5048−5079.
(13) Blochl, P. E. *Phys. Rev. B* **1994**, *50*, 17953−17979.
(14) Nikitin, A.; Naslund, L.; Nilsson, A. Unpublished work, 2007.
(15) Ruffieux, P.; Groning, O.; Schwaller, P.; Schlapbach, L.; Groning, P. *Phys. Rev. Lett.* **2000**, *84*, 4910−4913.
(16) Lu, G.; Scudder, H.; Kioussis, N. *Phys. Rev. B* **2003**, *68*, 205416.
(17) Zhang, G.; Qi, P.; Wang, X.; Lu, Y.; Mann, D.; Li, X.; Dai, H. *J. Am. Chem. Soc.* **2006**, *128*, 6026−6027.
(18) Zhang, G.; Qi, P.; Wang, X.; Lu, Y.; Li, X.; Tu, R.; Bangsaruntip, S.; Mann, D.; Zhang, L.; Dai, H. *Science* **2006**, *314*, 974−977.
(19) Kanai, C.; Watanabe, K.; Takakuwa, Y. *Phys. Rev. B* **2001**, *63*, 235311.
(20) Tanuma, S.; Powell, C. J.; Penn, D. R. *Surf. Interface Anal.* **2005**, *37*, 1−14.
(21) Zhang, Z.; Cho, K. *Phys. Rev. B* **2007**, *75*, 075420.
(22) Gulseren, O.; Yildirim, T.; Ciraci, S. *Phys. Rev. B* **2002**, *66*, 121401.
(23) Park, K. A.; Seo, K.; Lee, Y. H. *J. Phys. Chem. B* **2005**, *109*, 8967−8972.
(24) Nilsson, A. *J. Electron Spectrosc. Relat. Phenom.* **2002**, *126*, 3−42.
(25) Weiss, K.; Ostrom, H.; Triguero, L.; Ogasawara, H.; Garnier, M. G.; Pettersson, L. G. M.; Nilsson, A. *J. Electron Spectrosc. Relat. Phenom.* **2003**, *128*, 179−191.
(26) Hornekær, L.; Šljivančanin, Ž.; Xu, W.; Otero, R.; Rauls, E.; Stensgaard, I.; Lægsgaard, E.; Hammer, B.; Besenbacher, F. *Phys. Rev. Lett.* **2006**, *96*, 156104.
(27) Park, S.; Srivastava, D.; Cho, K. *Nano Lett.* **2003**, *3*, 1273−1277.
(28) Lueking, A. D.; Yang, R. T. *Appl. Catal., A* **2004**, *265*, 259−268.
(29) Lee, Y.-W.; Clemens, B. M. *Appl. Phys. J.*, submitted for publication, 2007.
(30) DOE FreedomCAR Hydrogen Storage Technologies Roadmap, http://www1.eere.energy.gov/vehiclesandfuels/pdfs/program/hydrogen_storage_roadmap.pdf (accessed November 13, 2007).

NL072325K